Click Here for Full Article

Influence of volcanic history on groundwater patterns on the west slope of the Oregon High Cascades

Anne Jefferson,[1] Gordon Grant,[2] and Tim Rose[3]

[1] Spring systems on the west slope of the Oregon High Cascades exhibit complex relationships among modern topography, lava flow geometries, and groundwater flow patterns. Seven cold springs were continuously monitored for discharge and temperature in the 2004 water year, and they were periodically sampled for $\delta^{18}O$, δD, tritium, and dissolved noble gases. Anomalously high unit discharges suggest that topographically defined watersheds may not correspond to aquifer boundaries, and oxygen isotope data reveal that mean recharge elevations for the springs are coincident with extensive Holocene lava fields. The $^3He/^4He$ ratios in most of the springs are close to atmospheric, implying shallow flow paths, and aquifer thicknesses are estimated to be $30–140$ m. Estimates using $^3H/^3He$ data with exponential and gamma distributions yield mean transit times of $\sim3–14$ years. Recharge areas and flow paths are likely controlled by the geographic extent of lava flows, and some groundwater may cross the Cascade crest.

Citation: Jefferson, A., G. Grant, and T. Rose (2006), Influence of volcanic history on groundwater patterns on the west slope of the Oregon High Cascades, *Water Resour. Res.*, *42*, W12411, doi:10.1029/2005WR004812.

1. Introduction

[2] The Cascade Range, an active volcanic arc stretching from southern British Columbia to northern California, intercepts Pacific Ocean air masses moving east over the northwestern United States. These moisture-rich air masses supply abundant precipitation to the western slopes of the Cascades, yielding runoff to major river systems in the Pacific Northwest. The topography of the Cascade Range is shaped by competing forces of constructional volcanism and glacial and fluvial erosional processes. In regions where volcanic effusion rates exceed erosion rates, thick undissected platforms of layered lava and pyroclastic flows dominate the landscape. In central Oregon, coalescing Quaternary age shield volcanoes produced a >1000 m thick sequence of basaltic lava flows in the fault-bounded High Cascades [*Conrey et al.*, 2002]. These young lavas have extremely high permeabilities [*Saar and Manga*, 2004], and a significant portion of the precipitation in this area infiltrates to recharge groundwater flow systems. These groundwater systems emerge down gradient as large-volume spring-fed streams with higher summer flows and lower temperatures than the shallow subsurface flow fed streams draining the adjacent, older, less permeable Western Cascades terrain [*Tague and Grant*, 2004; *Tague et al.*, 2006].

[3] Understanding the movement of water in this young volcanic landscape gives us insight into the interplay between volcanic history and groundwater resources that can be applied to other mafic volcanic regions, such as Iceland, Central America, and the East African Rift zone. In addition, heightened interest in understanding the history of water and channel development on Mars is focusing on similar interactions between groundwater and volcanism [*Aharonson et al.*, 2002; *Head et al.*, 2003].

[4] Furthermore, knowledge of Oregon Cascades hydrogeology is important for making water resource management decisions and predicting the response to potential changes in climate. Cascade rivers support salmon runs, generate hydropower, provide recreational opportunities, and supply drinking water to millions of people. In the summer, the majority of water from the Cascades is supplied by spring-fed streams from the young volcanic terrains of the High Cascades [*Gannett et al.*, 2003; *Jefferson et al.*, 2004]. As climate warms and snowpacks decrease according to current trends and predictions [*Hayhoe et al.*, 2004; *Mote et al.*, 2005], hydrological modeling suggests that spring-fed streams will be subject to declines in late summer discharge even as they become ever more important regional water resources (C. Tague et al., Deep groundwater mediates streamflow response to climate warming in the Oregon Cascades, submitted to *Climatic Change*, 2006).

[5] Hydrogeologic investigations of High Cascades aquifer systems are complicated by several factors. Surface runoff is largely absent, drainage density is low (~0.4 km/km^2) and there are few wells to provide hydraulic conductivity and head data. Multiple, overlapping volcanic centers with a several million year eruption history, punctuated by episodes of glaciation and erosion, preclude the application of models developed for shield volcanoes on ocean islands [e.g., *Izuka and Gingerich*, 2003; *Join et al.*, 2005]. Older lava flows were confined by topography that is now buried and obscured, resulting in hidden groundwater

[1]Department of Geosciences, Oregon State University, Corvallis, Oregon, USA.
[2]Pacific Northwest Research Station, Forest Service, U.S. Department of Agriculture, Corvallis, Oregon, USA.
[3]Chemical Biology and Nuclear Science Division, Lawrence Livermore National Laboratory, Livermore, California, USA.

divides and flow paths, but the size and inaccessibility of the area make geophysical methods for revealing aquifer structure impractical [e.g., *Descloitres et al.*, 1997; *Revil et al.*, 2004; *Join et al.*, 2005]. Flow paths may include flow both in fractures and through the porous matrix (a dual porosity system), providing spring systems in this area with complex timescales of response to changes in recharge [*Manga*, 1999].

[6] In this study we use springs as a window into the subsurface hydrology of the High Cascades and apply a variety of methods to investigate the source, quantity, and transit time of the water. Additionally, we examine the congruence of subsurface flow paths and surface topography, and estimate hydraulic conductivities. We report discharge and temperature measurements, derive recharge elevations from stable isotopes, estimate flow path depths and transit times with tritium and noble gases, and predict recharge areas using mass balance and lava flow geometry for seven groundwater systems in the McKenzie River watershed. Our intent is to both expand understanding of this important source of water in the Pacific Northwest and to explore interactions between volcanic and hydrogeologic processes.

2. Geologic and Hydrologic Context

[7] The active portion of the Oregon Cascades volcanic arc, formed by the subduction of the Juan de Fuca plate under the North American plate, is a partially fault-bounded region known as the High Cascades. Rift related volcanism associated with nearly 3 km of subsidence within the High Cascades over the last 5 million years has resulted in the eruption of dominantly basaltic and basaltic andesite lavas [*Conrey et al.*, 2002]. These eruptions have generated a thick pile of relatively flat lying mafic lava flows and cinders, punctuated by composite volcanoes such as the Three Sisters. The study area lies at the convergence of the Cascade volcanic arc, Basin and Range, and High Lava Plains (Figure 1a). The central Oregon Cascades has experienced the most extensive Quaternary mafic volcanism of any part of the arc [*Sherrod and Smith*, 1990]. The area has also been subject to three Pleistocene glaciations, which formed ice caps and valley glaciers [*Scott*, 1977], and whose deposits obscure some of the older volcanic rocks. To the west of the High Cascades lie the Western Cascades, a 10- to 40-million-years-old mature continental arc, dominated by voluminous dacitic tuffs, andesitic lava flows and minor basaltic and rhyolitic volcanic rocks.

[8] The geologic differences between the High Cascades and the Western Cascades result in distinct landscape forms and hydrologic functioning (Figure 1b). The High Cascades landscape has relatively gentle slopes, with little dissection, and it is underlain by young, high-permeability rocks of relatively uniform composition. The Western Cascades landscape is steep, deeply dissected, and underlain by older, low-permeability rocks of varying compositions. High Cascades stream networks are primarily spring fed, whereas Western Cascade streams are runoff dominated.

[9] Of the numerous High Cascades volcanic centers, several bear special note in reference to the hydrology of the study area (Figure 1c). Scott Mountain is a late Pleis-

tocene basaltic shield volcano with 32 km^2 of exposed lava and more extensive lava flows covered by till [*Conrey et al.*, 2002]. Eruptions from Belknap Crater covered 63 km^2 with lava between ∼3000 and 1300 years before present (ybp), while the Sand Mountain-Nash Crater chain of 23 cinder cones and associated lava flows covered 68 km^2 between ∼3800 and 2750 ybp [*Sherrod et al.*, 2004]. Sims Butte and Collier Cone have sent basaltic andesite lava down the Lost Creek glacial trough in the past 15,000 years [*Conrey et al.*, 2002]. South of the Three Sisters, volcanism on the west side of the crest has been quiet for >120,000 years, and glaciation and erosion have made determination of individual vents and associated flows more difficult [*Sherrod*, 1991]. However, one of our major cold springs issues from these Quaternary lavas.

[10] The McKenzie River watershed (Figure 1c) drains the west side of the High Cascades from Three Fingered Jack to south of the Three Sisters. In this watershed, seven springs with discharge >0.85 m^3/s have been identified. Six of these springs drain into tributaries of the McKenzie River above McKenzie Bridge, Oregon. At McKenzie Bridge, the McKenzie River has a topographic drainage area of 901 km^2, of which 507 km^2 are covered by Quaternary volcanic rocks. The remaining large spring is on a tributary to the South Fork of the McKenzie River. In most of the study area, a normal fault with >1 km offset separates the High Cascades from the Western Cascades [*Conrey et al.*, 2002]. The upper portion of the McKenzie River parallels this fault line.

[11] In the High Cascades, >75% of the annual precipitation falls during the winter. Midlatitude storms rise over the Cascades, resulting in a strong orographic effect. Above 1500 m, most precipitation falls as snow, which remains until the late spring. Below 1500 m, precipitation falls as both rain and snow, and snowpacks are transient. The west side receives ∼2.00 to 3.80 m of rain and snow per year, compared with ∼0.75 to 1.65 m of precipitation, predominantly snow, on the eastern slope [*Taylor and Hannan*, 1999]. The 2003 and 2004 water years had slightly below normal precipitation, with 89 and 93%, respectively, of the 1971−2000 mean annual precipitation.

[12] Long-term streamflow records are sparse in the High Cascades, and most of the USGS gauges in the McKenzie River watershed are along the main stem (Figure 1c). Generally, High Cascade streams exhibit muted winter peak flows and nearly constant summer base flows, with peak flows only 3−4 times higher than summer flows. In contrast, streams in other parts of western Oregon have peak flows >1000 times higher than base flows [*Tague and Grant*, 2004]. Geothermal spring systems are present along faults on the western slope of the Cascades (Figure 2) [*Ingebritsen et al.*, 1994], but are volumetrically minor contributors to streamflow.

[13] An array of isotopic studies, discharge measurements, and hydrogeologic models have been employed to gain insight into volcanic aquifers on the east side of the Cascade crest [*Manga*, 1996, 1997, 1998; *Manga*, 1999; *James et al.*, 2000; *Gannett and Lite*, 2004; *Manga and Kirchner*, 2004], but different dynamics might apply to the western slope of the Cascades due to the greater precipitation flux, which could lead to shorter transit times or greater water storage than on the east side. Also, on the western
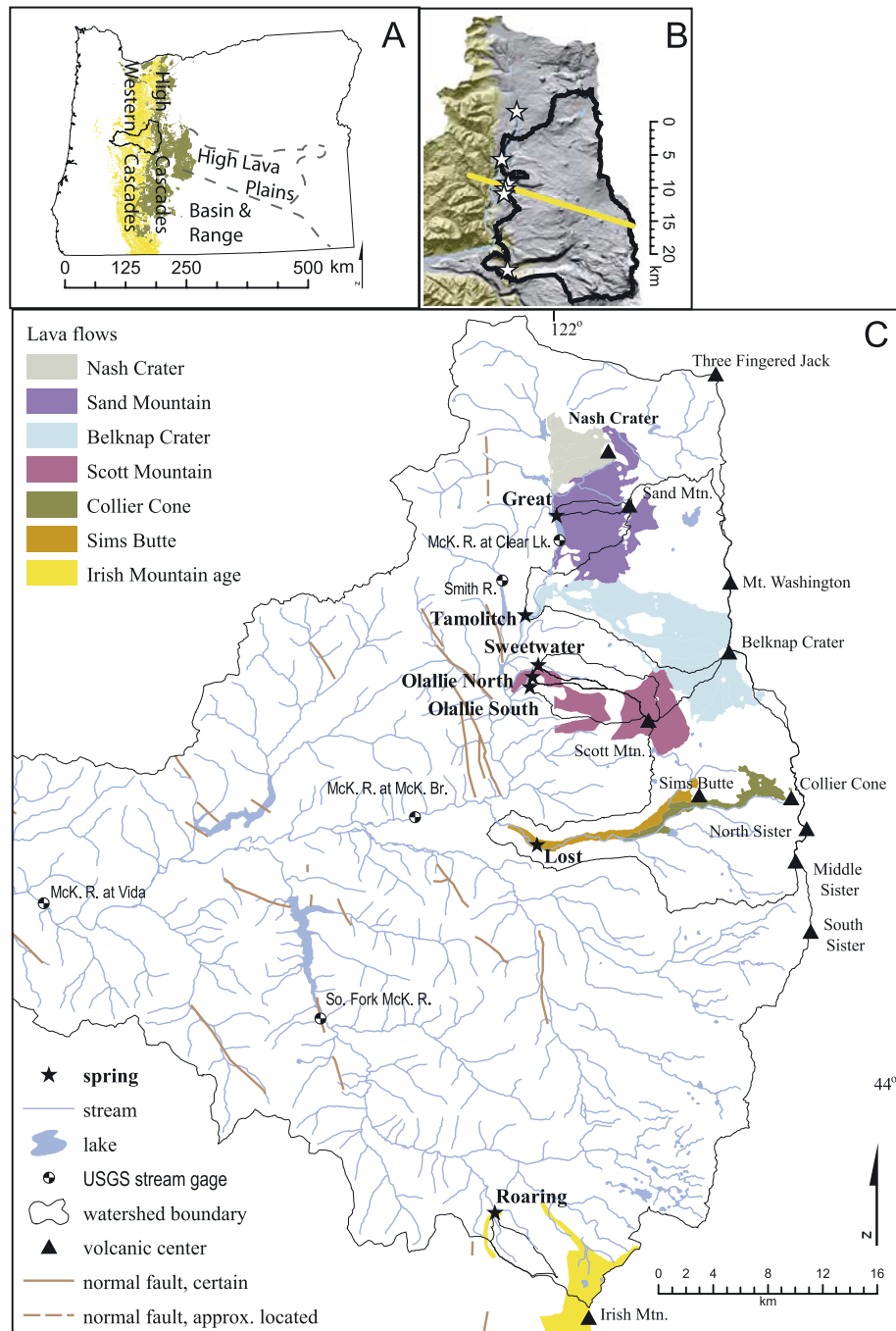
Figure 1. (a) Extent of High Cascade and Western Cascade volcanic rocks in Oregon [*Sherrod and Smith*, 2000], with the McKenzie River watershed (black outline) and some adjacent physiographic regions for reference. (b) Topography of the upper portion of the McKenzie River watershed showing Western Cascade geology (shading), locations of springs (stars), the cross-section illustrated in Figure 2 (light line), and the area discussed in section 5.1 (black outline). (c) Locations of hydrologic and geologic features referred to in text. The McKenzie River watershed forms the map boundary. In the vicinity of Irish Mountain, depicted lava is undifferentiated 120,000–780,000 basalt and basaltic andesite. Geology is based on the work of *Sherrod and Smith* [2000] and *Sherrod et al.* [2004]. Lost Spring's watershed is calculated below the spring, where the stream channel is single thread.

slope, the mixture of rain and snow creates multiple pulses of recharge. Additionally, Quaternary lavas on the west side of the Cascades are bounded <15 km from the crest by higher-elevation and lower-permeability Western Cascades rocks, whereas on the east side, High Cascades lavas commingle with high-permeability back arc and Basin and Range volcanic rocks at comparable elevation. Thus flow paths are likely on the order of kilometers on the west side
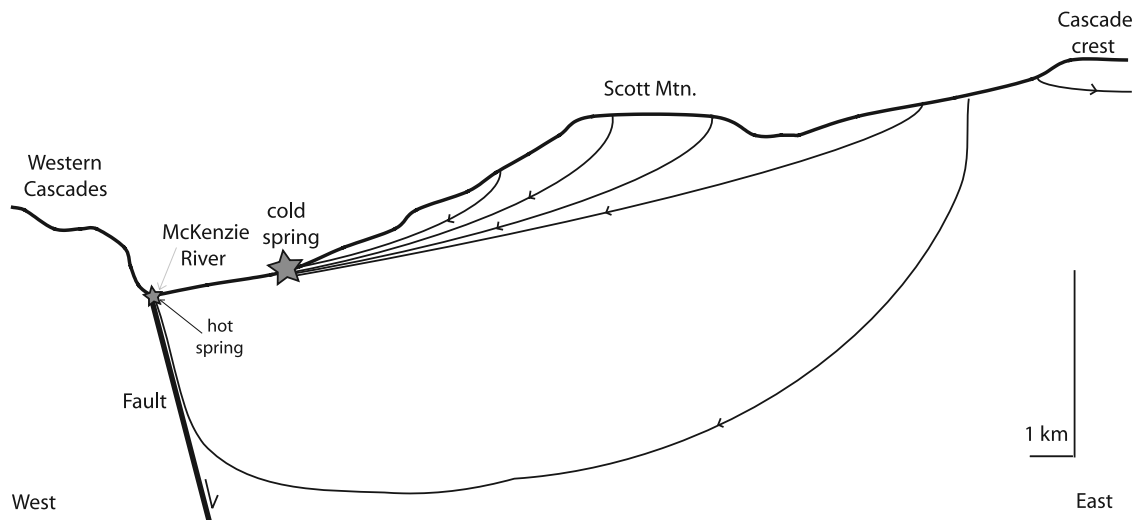
Figure 2. Cross section from the Cascade crest to the Western Cascades along the line in Figure 1b. Actual topography is shown, but flow paths are conceptual. Hot springs occur where deep groundwater flow paths are interrupted by faults [*Ingebritsen et al.*, 1994], while cold springs are the result of shallower flow paths.

rather than tens of kilometers as on the east side [*James et al.*, 2000].

3. Methods

3.1. Study Site Selection and Characterization

[14] A survey of discharge measurements revealed that the majority of summer flow in the McKenzie River is sourced at springs, and seven of the largest springs were selected for detailed study. For the 2004 water year (10/1/2003 to 9/30/2004), we monitored discharge at Lost, Olallie North, Olallie South, Roaring, and Sweetwater springs (Figure 1c and Table 1). TruTrack WT-HR data loggers were used to measure water height at 15- to 60-min intervals, and discharge was measured >10 times at each site using a Marsh-McBirney velocity meter via wading [*Carter and Davidian*, 1968]. Stage-discharge rating curves were developed to calculate mean annual discharge. Beginning in July 2002, water temperature was measured hourly at each of the springs by Onset Hobo[®] Water Temp Pro data loggers, with ±0.2°C accuracy.

[15] The other two large springs are Tamolitch and Great Springs. Gauging downstream of Tamolitch Spring was established in October 2003 by Stillwater Sciences. Great Spring feeds directly into Clear Lake, which is gauged by the USGS (gauge 14158500). Clear Lake has many springs and seeps along the lakeshore and bottom, of which Great Spring is the most easily accessible. Groundwater is the only source of August flow from Clear Lake, and it averages 8.5 m^3/s [*Herrett et al.*, 2004], of which Great Spring contributes 10% [*Stearns*, 1929].

[16] We computed a simplified water balance for the 2004 water year for the topographic watersheds of the springs. Topographic watersheds were delineated from a 10-m DEM using ArcGIS9. Monthly values of precipitation in 2 km by 2 km grid cells were derived from the PRISM model [*Daly et al.*, 1994, 2002] and summed. A runoff ratio, which is the fraction of precipitation that results in streamflow, of 0.68 was calculated for the McKenzie River near Vida, and was used as a regional value to constrain evapotranspiration. Evapotranspiration is recognized to vary with vegetation and altitude, but distributed data do not exist for the study

Table 1. Attributes of Springs

	Great	Lost	Olallie North	Olallie South	Roaring	Sweetwater	Tamolitch
Topographic watershed area, km^2	3.88	197	2.96	15.9	9.03	14.8	127
Spring elevation, m	918	585	715	630	1100	725	725
Mean discharge, m^3/s	0.85[a]	6	1.7	2.3	1.9	1.6	4.1[b]
Mean temperature, °C	4.9	6.3	4.5	5.1	4.5	4.6	5.4
Temperature standard deviation, °C	0.12	0.54	0.03	0.01	0.07	0.12	0.09
Number of days with temperature data	519	643	778	853	800	243	98
Mean $\delta^{18}O$, ‰	−12.8	−12.9	−12.6	−12.3	−13	−12.7	−12.6
$\delta^{18}O$ standard deviation, ‰	0.46	0.10	0.05	0.03	0.05	0.05	0.11
Number of $\delta^{18}O$ samples	11	23	22	6	6	3	6
Mean recharge elevation, m	1372	1472	1247	1072	1528	1353	1278
Estimated recharge area, km^2	20.2	114	30.7	50.5	48.1	32.4	74.1
GPE dissipation corrected temperature, °C	3.9	4.3	3.3	4.1	3.5	3.2	4.1

[a]*Stearns* [1929].
[b]Data provided by Stillwater Sciences.

area, so here we neglect spatial variability. We assumed that the 2409 km^2 drainage area of the McKenzie River above Vida is large enough that slight discrepancies between the topographically defined watershed and the groundwater recharge areas are probably insignificant to the calculated runoff ratio. Runoff ratios were also calculated for three smaller sub basins of the McKenzie River that are gauged by the USGS. These basins had ratios ranging from 0.63 to 0.76, supporting the use of the runoff ratio at Vida as a reasonable regional value.

3.2. Sample Collection and Analysis

[17] In order to determine source areas for the lava found at springs, rock samples were collected at four of the springs. Bulk rock samples were analyzed via X-ray fluorescence at Washington State University's GeoAnalytical Laboratory for 27 major and trace elements. These data were compared to each other and published rock chemistries.

[18] Stable isotope data for 174 samples of springs, streams, lakes, and precipitation from the McKenzie River watershed were collected and analyzed between July 2002 and March 2005. Each of the seven major springs was sampled for stable isotopes at least three times, with two springs (Olallie North Spring and Lost Spring) sampled repeatedly (n = 22) to establish long-term trends in isotopic composition. Isotopic sample preparation was by the water-CO_2 equilibration method [Epstein and Mayeda, 1953] for oxygen isotopes, and by the zinc reduction method for deuterium [Coleman et al., 1982]. Analyses were completed on a VG dual inlet isotope ratio mass spectrometer at Lawrence Livermore National Laboratory. Isotopic values are reported in the standard δ notation as per mil (‰) deviations from the VSMOW reference standard.

[19] Water samples were collected at six of the major springs in August 2004 for helium and tritium analysis. Samples for helium analysis were collected in copper tubes, which were submersed in the spring pool, tapped to dislodge trapped air bubbles, and sealed with stainless steel pinch-off clamps. Samples for tritium analysis were collected in plastic bottles. Tritium and helium analyses were completed by the Noble Gas Isotope Lab at the University of Miami, following procedures described by Clarke et al. [1976]. All samples were collected as close as possible to the spring orifice, as noted by water bubbling or gushing from the rocks.

3.3. Recharge Elevation Estimation

[20] In mountainous regions, precipitation becomes progressively depleted in heavy isotopes (^{2}H and ^{18}O) with increasing elevation, as first described by Dansgaard [1964]. In this study, the variation in stable isotope values of small springs as a function of altitude was used to estimate the average recharge elevations for large springs. Small springs are considered proxies for local recharge of precipitation at a given elevation [Rose et al., 1996]. Samples from 10 small springs (<0.12 m^3/s discharge) were collected during the summers of 2003 and 2004. Additionally, data from 9 small springs and 1 well from the McKenzie River watershed, or drainages to the west, were reported by Ingebritsen et al. [1994], and data were used from 7 springs sampled by Evans et al. [2004] from the McKenzie watershed.

3.4. Helium Calculations and Transit Time Estimation

[21] The time from when water enters an aquifer to when it exits at a spring is referred to as the transit time [Etcheverry and Perrochet, 2000]. Tritium (^{3}H) and tritogenic helium (^{3}He$_{trit}$) have been employed to date young groundwater (transit times less than ~50 years) in a variety of settings [Aeschbach-Hertig et al., 1998; James et al., 2000; Rademacher et al., 2005]. Atmospheric tritium concentrations greatly increased as a result of nuclear weapons testing in the 1950s and 1960s, but by the 1990s, atmospheric tritium activities had approximately returned to prebomb levels. The constrainable time period and resolution are enhanced by measuring ^{3}H in combination with its daughter product, ^{3}He$_{trit}$.

[22] All of the tritium in groundwater is derived from the atmosphere, but helium has multiple sources that complicate interpretation. In order to constrain the amount of ^{3}He$_{trit}$ in a water sample, it is necessary to determine the contributions from atmosphere equilibrium solubility, dissolution of air bubbles during recharge (so called "excess air"), decay of U and Th in the crust, and mantle helium from magmatic sources. Crustal and mantle sources of helium are referred to as terrigenic. Fortunately, atmospheric, crustal, and mantle sources have differing ratios of ^{3}He/^{4}He, and all neon is commonly assumed to be atmospherically derived, so these differences can be used to calculate the relative contribution of helium from each source [Schlosser et al., 1989].

[23] Following Schlosser et al. [1989], terrigenic helium (^{4}He$_{terr}$) is derived from

$$^4He_{terr} = {}^4He_{meas} - \left(\frac{^4He}{Ne}\right)_{atm} \cdot (Ne_{meas} - Ne_{eq}) - {}^4He_{eq}, \quad (1)$$

where ^{4}He$_{meas}$ is the measured helium concentration, (^{4}He/Ne)$_{atm}$ is 0.2882 [Hilton, 1996], Ne$_{meas}$ is the measured neon concentration, Ne$_{eq}$ is the equilibrium dissolved neon concentration, and ^{4}He$_{eq}$ is the equilibrium dissolved helium concentration. Equilibrium solubilities of Ne and He were corrected for recharge temperature and altitude. Recharge temperature is assumed to be the same as the spring temperature corrected for gravitational potential energy dissipation [Manga and Kirchner, 2004], as discussed below, and mean recharge altitude is derived from δ^{18}O values of the springs as described above.

[24] Total ^{3}He is calculated by multiplying the measured ^{4}He concentration by the measured ratio of ^{3}He to ^{4}He. The atmospheric ^{3}He component, which includes both equilibrium and excess helium, is determined using

$$^3He_{atm} = \left({}^4He_{meas} - {}^4He_{terr}\right) \cdot R_a - {}^4He_{eq} \cdot R_a \cdot (1 - \alpha), \quad (2)$$

where R_a is the atmospheric ^{3}He/^{4}He ratio, 1.384×10^{-6} [Clarke et al., 1976], and $\alpha = 0.983$, the solubility isotope effect [Schlosser et al., 1989]. Tritogenic helium is calculated as

$$^3He_{trit} = {}^4He_{meas} \cdot \left(\frac{^3He}{^4He}\right)_{meas} - {}^3He_{atm} - {}^4He_{terr} \cdot \left(\frac{^3He}{^4He}\right)_{terr},$$
$$(3)$$

where (^{3}He/^{4}He)$_{meas}$ is the measured helium isotope ratio and (^{3}He/^{4}He)$_{terr}$ is the terrigenic helium isotope ratio.

[25] It is common to assume that either mantle or crustal sources of helium can be neglected in the terrigenic helium flux when using the tritium-helium method to date groundwater [e.g., *Schlosser et al.*, 1989; *James et al.*, 2000], because the terrigenic helium isotope ratio cannot be measured directly in environments where both mantle and crustal helium are expected to occur. Following *Saar et al.* [2005], we consider mantle helium in the Cascades to have an $^3He/^4He$ ratio normalized to the atmosphere (R/R_a) of 8.19 and crustal helium to have $R/R_a = 0.007$. We solve equation (3) by varying $(^3He/^4He)_{terr}$ iteratively until the resultant $^3He/^4He$ ratio, including the atmospheric, terrigenic, and tritogenic components, equals the measured $^3He/^4He$ ratio of each sample.

[26] Once tritogenic helium concentrations are obtained, $^3H/^3He$ mean transit time (T) is calculated using

$$T = \frac{t_{1/2}}{\ln 2}\left[1 + \frac{^3He_{trit}}{^3H}\right],$$ (4)

where $t_{1/2}$ is the tritium half-life (12.43 years) and $^3He_{trit}$ and ^3H are expressed in tritium units [*Schlosser et al.*, 1989]. Uncertainty in the transit time estimates is the result of measurement uncertainty in the tritium concentrations and uncertainty in the correct recharge temperature and elevation.

[27] Equation (4) inherently calculates transit times with a piston flow model. *Manga* [1999] suggested that High Cascades aquifers are more appropriately modeled with an exponential transit time distribution, which incorporates distributed recharge and mixing of water of different ages at the spring orifice. The transit time distribution, g(t), for this model,

$$g(t) = \frac{1}{T}e^{t/T},$$ (5)

is a function of time (t), and the mean transit time (T). Work by Kirchner and others [2001], suggests that many catchments do not exhibit behavior consistent with the exponential model. Their work supports a gamma transit time distribution,

$$g(t) = \frac{\tau^{\alpha-1}}{\beta^\alpha \Gamma(\alpha)}e^{-\tau/\beta},$$ (6)

where β is a scale parameter and α is a shape parameter. Mean transit time is $\alpha\beta$, and $\alpha \sim 0.5$ has been found to fit solute tracer concentration curves for a number of catchments [*Kirchner et al.*, 2001].

[28] These transit time distributions are implemented using the convolution integral,

$$c_{out}(t) = \int_{-\infty}^{t} c_{in}(\tau)g(t-\tau)e^{-\lambda(t-\tau)}d\tau,$$ (7)

where c_{out} and c_{in} are the output and input time series, τ is an integration variable, and λ is the radioactive decay constant. The input time series is provided by precipitation-weighted tritium concentrations at Portland which began in

1963 (IAEA/WMO, The GNIP Database, Global Network of Isotopes in Precipitation, http://isohis.iaea.org/), and extended backward to 1953 by regression with measurements made in Ottawa [*Michel*, 1989]. The convolution integral was used with both exponential and gamma transit time distributions and solved for yearly time steps of 0 to 50 years using the 2004 output concentrations of ^3H and ^3He. The $^3H/^3He$ mean transit times were derived by linearly interpolating between the closest time steps of ^3H and ^3He transit times.

4. Results

4.1. Recharge Areas

[29] The seven major spring systems all have runoff ratios that diverge from the regional average (Figure 3). Five of the springs discharge more water than their topographic watersheds receive in precipitation, as shown by the position above the 1:1 line. In order to account for the high discharge values, these springs must be receiving water sourced outside their topographic watersheds. Conversely, the two springs that plot below the regional average are not receiving all of the precipitation that falls on their topographic watershed. Thus, there is a strong discordance between topographic watersheds and groundwater recharge areas. These results suggest that modern topography is not the main constraint on groundwater catchments, despite relief of ~1000 m between the elevation of the springs and the Cascade crest. Given this finding, we used stable isotopes, water temperature, and rock chemistry to provide insights into recharge elevations and areas for the springs.

[30] We derived a local meteoric water line of $\delta D = 8.3\ \delta^{18}O + 17$ ($r^2 = 0.95$, n = 44) based on isotopic sampling of springs, streams, and precipitation in the McKenzie River basin (Figure 4). Evaporative enrichment was only exhibited by late summer samples from small spring pools and lakes (not shown in Figure 4). Thus evaporation does not appear to have significantly affected the isotopic composition of the snowpack, or that of infiltration through the unsaturated zone.

[31] Repeated sampling (n = 22) of Lost Spring and Olallie North Spring from July 2002 to March 2005 showed little variability in isotopic composition on a seasonal or interannual basis (Figure 5). The standard deviation for the Lost Spring data set was 0.08‰, and for Olallie North Spring it was 0.05‰. Both of these values are smaller than the analytical uncertainty of 0.1‰. Given an annual range of precipitation $\delta^{18}O$ of 8‰, based on a 3-year record from a Western Cascades site <10 km west of the upper McKenzie River [*McGuire et al.*, 2005], the lack of variability in the groundwater suggests complete mixing at the spring orifice or that transit times may be long enough to substantially mute input variability.

[32] Small springs show a decrease in $\delta^{18}O$ of 0.16‰ per 100 m elevation gain, as shown in Figure 6 ($r^2 = 0.67$), which is slightly lower than temperate and worldwide averages of 0.20‰ per 100 m elevation gain [*Dansgaard*, 1964; *Bowen and Wilkinson*, 2002], but is within the 0.14 to 0.23‰ range of values reported for the Cascade Range [*Ingebritsen et al.*, 1994; *Rose et al.*, 1996; *James et al.*, 2000; *Nathenson and Thompson*, 2003].
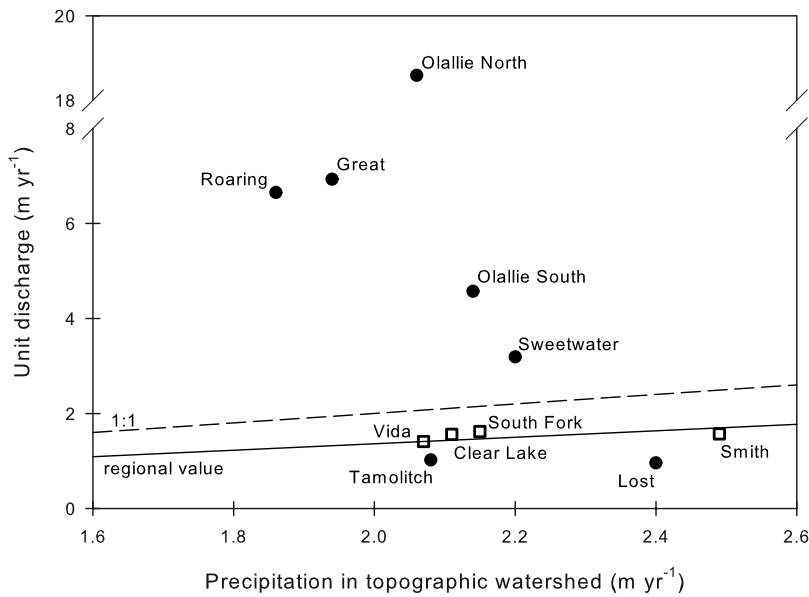
Figure 3. Relationship between unit discharge and precipitation for springs (circles) and USGS gauges (squares) for water year 2004. The regional value line represents the runoff ratio for the McKenzie River at Vida (0.68). USGS gauges aggregate both spring-fed and runoff-dominated streams.

[33] The altitude-isotope line (Figure 6) was fitted by linear regression to the isotopic compositions and discharge elevations of the small springs. Even though small springs are assumed to recharge locally, there is some recharge elevation above their outlets. Local peaks were generally less than 150 m higher than the small springs, and the springs are likely recharging water at multiple elevations along the slopes. Unambiguous recharge elevations could not be definitively identified from the surrounding topography, so discharge elevations were used instead. Given the slope of the altitude-isotope line, uncertainty in recharge elevations associated with analytical error of isotope values is ±60 m. Uncertainty associated with recharge elevations is probably on the same order of magnitude.

[34] Projecting the mean isotopic composition of large springs (Table 1) onto the altitude-isotope line for small springs, recharge-weighted mean recharge elevations were found to be between 1000 and 1600 m (Figure 7). The elevation range for recharge to the springs corresponds with the majority of the area covered by Quaternary mafic lava.

[35] Like $\delta^{18}O$, temperature has also been used as a proxy for recharge elevation, although its interpretation may be
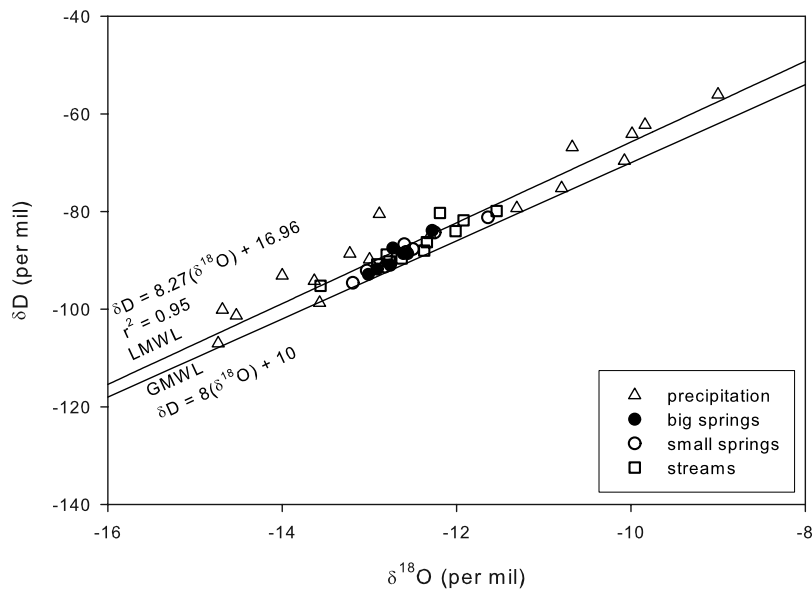

Figure 4. Relationship between $\delta^{18}O$ and δD for springs, streams, and precipitation in the McKenzie River watershed for samples collected in this study. GMWL is the global meteoric water line [*Craig*, 1961], and LMWL is the local meteoric water line, representing the best fit through the data. Points represent averages of all data for each site.
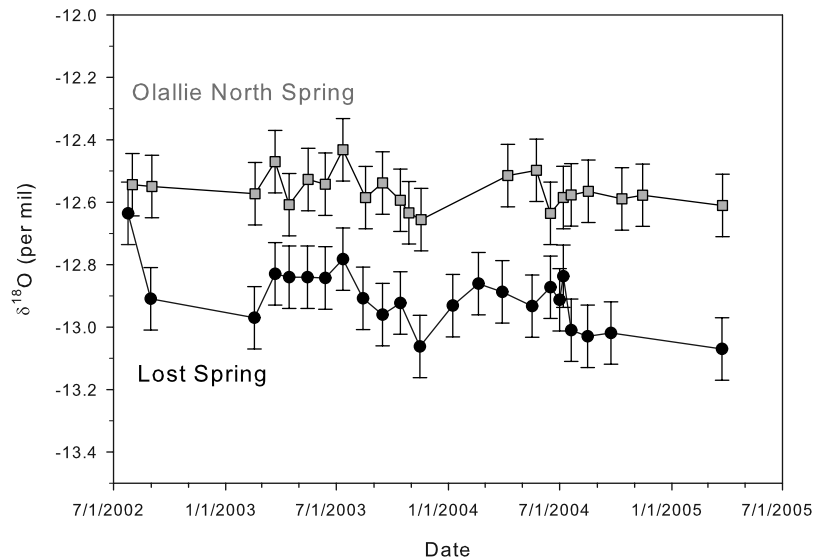
Figure 5. Time series of $\delta^{18}O$ data for two large springs, with analytical error bars of 0.1‰. The annual range in precipitation $\delta^{18}O$ for a nearby watershed was 8‰ for the years 2000–2002 [*McGuire et al.*, 2005].

complicated by geothermal heating and the dissipation of gravitational potential energy. *Manga and Kirchner* [2004] suggest that such dissipation is a significant heat source for springs in volcanic regions, citing energy balance calculations and examples from Mt. Shasta in California and the east side of the Oregon High Cascades. Given their findings, we compared spring temperatures to the mean annual surface temperature of their isotopically inferred recharge elevations. Mean annual and mean May temperature data were obtained for 10 stations on the west slope of the Cascades in the vicinity of the study area from the Oregon Climate Service, H.J. Andrews Experimental Forest, and Natural Resources Conservation Service SNOTEL network.

A best fit line for mean annual temperature was $-5.7°C/km + 13.6$ ($r^2 = 0.80$), and May temperatures, during the principal snowmelt and groundwater recharge period, were higher than mean annual temperatures. Measured temperatures at six of seven springs were equal to or lower than mean annual surface temperatures for the mean recharge elevations. When the correction for gravitational potential energy (2.3°C/km [*Manga and Kirchner*, 2004]) is applied, all springs are 0.9–3.4°C colder than their recharge elevations. Measured temperature at Lost Spring is warmer than predicted for its mean recharge elevation, but colder when corrected for gravitational potential energy. As discussed below, temperature at this spring may be influenced by
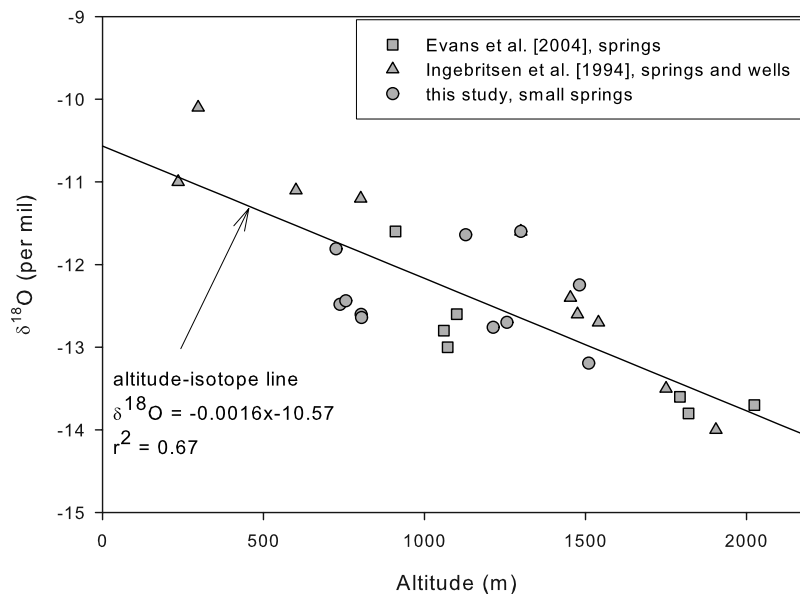
Figure 6. Relationship between altitude and $\delta^{18}O$ for small springs and wells, within and west of the study area. Altitude-isotope line is a regression through small spring data from this study along with data from *Ingebritsen et al.* [1994] and *Evans et al.* [2004] for small springs and wells.
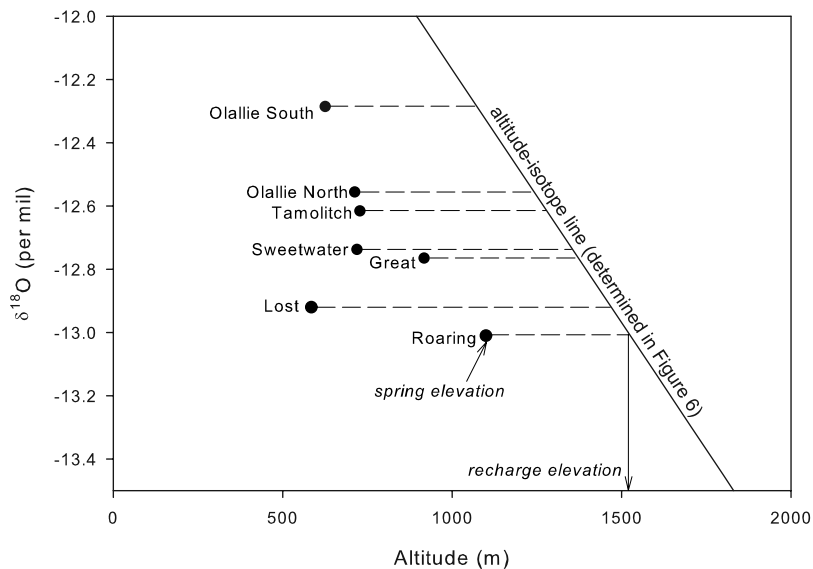
Figure 7. Calculation of mean recharge elevations, based on the altitude-isotope line determined in Figure 6 and average $\delta^{18}O$ of the large springs. Recharge elevations are determined by extrapolating the average $\delta^{18}O$ of each spring to the altitude-isotope line and dropping a perpendicular to the x axis.

mixing with geothermal water. Therefore geothermal heating appears to be insignificant in most cases, and we suggest that springs are probably deriving their water from a range of elevations and associated recharge temperatures.

[36] We propose that the geometry of lava flows may have a dominant control on aquifer geometry. Basaltic lava flows have highly permeable rubble zones surrounding a dense, low-permeability interior [*Kilburn*, 2000]. Most water flow occurs within the rubble zones, but fractures allow transmission of water through flow interiors and vertically between lava flows [*Kiernan et al.*, 2003]. Rubble zones at contacts between lava flows result in highly anisotropic aquifers, with the direction of highest permeability oriented parallel to the lava flow direction [*Davis*, 1969]. These high-permeability regions are not laterally continuous between adjacent lava flows, potentially segregating groundwater flow paths by the spatial extent of a particular lava lobe. Volcanic dikes and lower-permeability strata can also compartmentalize groundwater flow [*Izuka and Gingerich*, 2003]. In the Cascades, most lava flows originate near the crest and flow primarily east or west, filling in lows in the preexisting topography. In many places, young lava flows abut older, more weathered, and potentially less permeable rocks. Thus, determining the source vent of a lava flow from which a spring issues allows the identification of probable recharge areas that may lie outside the spring's topographic watershed.

[37] Published geologic maps clearly link lava at the Great, Tamolitch, and Lost springs to their source vents (Figure 1c). Great Spring rises from Sand Mountain lava [*Sherrod et al.*, 2004], Tamolitch Spring emerges from Belknap Crater lava [*Stearns*, 1929], and Lost Spring springs from Sims Butte lava [*Lund*, 1977], so no rocks were collected or analyzed at these locations. The area around Sweetwater, Olallie North, and Olallie South springs has not been mapped in detail. A map of the Oregon Cascades shows the area around Sweetwater and Olallie South springs as unconsolidated sediments or sedimentary

rocks [*Sherrod and Smith*, 2000]. Nonetheless, upon reconnaissance, we found vesicular lava flows exposed and sampled them at the orifices of Sweetwater and Olallie North springs. Olallie South Spring emerges from beneath a talus pile, so the ridge above the spring and a downslope area were sampled instead.

[38] Trace elements can be particularly diagnostic for identifying rocks from the same lava flow or vent. Strontium and Nb are two trace elements commonly used to distinguish lavas in the Oregon Cascades [*Conrey et al.*, 1997]. Samples at Sweetwater and Olallie North have very similar Sr and Nb concentrations (Table 2), indicating that the rocks are likely part of the same lava flow. The sample downslope of Olallie South has a different major element composition but similar Sr and Nb concentrations compared to the Sweetwater and Olallie North samples. The sample from the ridge above Olallie South is clearly from a different source. These interpretations are supported by comparisons of major element variations including SiO_2, TiO_2, and the Mg# (molar ratio of Mg to Mg plus Fe). Sweetwater and Olallie North have identical Mg numbers of 0.60, while the downslope sample equals 0.59 and the ridge sample equals 0.57. The ridge sample also has more SiO_2 and less TiO_2 than the other samples (Table 2). The chemical compositions of the Sweetwater and Olallie North samples are very similar to that of a sample from near the summit of Scott Mountain. This sample (99-37) has 683 ppm Sr, 13.2 ppm Nb, 50.47 wt% SiO_2, and 1.60 wt% TiO_2, all of which closely correspond to the Sweetwater and Olallie North Samples [*Conrey et al.*, 2002].

[39] On the basis of the rock chemistry (Table 2), we interpret the Sweetwater and Olallie North samples as being part of the same Scott Mountain lava flow, and the sample downslope of Olallie South as also originating from Scott Mountain. This suggests that the Scott Mountain area is a likely source of recharge to Sweetwater and Olallie North springs. The ridge above Olallie South is not composed of

Table 2. XRF Analyses of Samples Collected in the Vicinity of Springs

| | Sweetwater Spring | Olallie North | Downslope of Olallie South | Ridge Above Olallie South | Roaring | |
					Above Spring	Below Spring
Sample	AJ-05-4	AJ-04-3	AJ-05-3	AJ-05-5	AJ-04-6	AJ-04-5
			Normalized Major Elements (wt %)			
SiO_2	50.5	50.4	50.13	51.91	55.06	54.89
TiO_2	1.688	1.672	1.665	1.403	1.104	1.113
Al_2O_3	17.05	17.1	17.08	17.77	18.21	18.23
FeO^*	9.16	9.05	9.52	9.06	7.86	7.91
MnO	0.156	0.156	0.163	0.163	0.141	0.142
MgO	7.56	7.62	7.7	6.65	4.82	4.85
CaO	9.12	9.08	9.11	8.55	7.52	7.64
Na_2O	3.34	3.47	3.33	3.46	4.12	4.09
K_2O	1.02	1.04	0.91	0.66	0.85	0.83
P_2O_5	0.403	0.407	0.388	0.377	0.316	0.32
			Unnormalized Trace Elements (ppm)			
Ni	133	136	144	136	73	70
Cr	220	223	229	217	99	98
Sc	27	27	28	26	21	20
V	205	203	199	204	171	172
Ba	382	395	370	366	386	393
Rb	11	8	9	6	10	9
Sr	667	662	646	502	611	617
Zr	158	148	154	158	109	109
Y	26	24	26	29	20	21
Nb	13.1	13.7	12.3	10.1	6	5.8
Ga	17	16	18	19	20	19
Cu	49	60	62	56	60	55
Zn	81	80	83	92	82	83
Pb	2	7	3	5	6	5
La	17	14	19	18	11	15
Ce	35	40	43	39	29	24
Th	2	2	1	1	3	1
Nd	21	28	23	23	18	16

Scott Mountain lava, and it is mapped as older Quaternary basaltic andesite not linked to any identified vent [*Sherrod and Smith*, 2000]. Olallie South Spring may be fed by a source other than or in addition to Scott Mountain.

[40] Spring water temperature and $\delta^{18}O$ data impart additional information about relationships between source areas for Sweetwater, Olallie North, and Olallie South springs. Sweetwater Spring and Olallie North Spring are located 952 m apart, but both emerge from Scott Mountain lava and their mean $\delta^{18}O$ and temperature are within analytical uncertainty of each other (Table 1). We conclude that Sweetwater and Olallie North springs are likely sourced in the same area. In contrast, Olallie South Spring, which is located 785 m south of Olallie North Spring, has water that is warmer by 0.6°C and isotopically heavier than Olallie North Spring. We conclude that Olallie South has a different, lower-elevation recharge area than Olallie North and Sweetwater springs.

[41] Roaring River is fed by Roaring Spring and a second 0.73 m³/s spring located ∼300 m north. As these two springs have temperature and $\delta^{18}O$ within analytical uncertainty of each other, we infer that they share the same water source. Roaring Spring issues from basaltic andesite that may have originated near Irish Mountain, but cannot be definitely linked to Irish Mountain based on published rock chemistry data. The orifice of Roaring Spring spans ∼50 m along a nearly horizontal line, but samples from lava both above and below the height of the Roaring Spring orifice

are within analytical uncertainty for many elements, and have very similar Sr and Nb concentrations (Table 2). On the basis of the rock chemistry, then, we conclude that the groundwater does not reach the land surface at Roaring Spring via a contact between lava flows. Instead the water may be discharging through a fracture network within a single flow.

[42] In the Lost Creek glacial trough, a spring with unusual discharge dynamics seems to share the same recharge area with the larger, perennial Lost Spring. Ephemeral White Branch Spring ($0 \leq Q \leq 2$ m³/s) is located 750 m up valley, but has the same mean $\delta^{18}O$ and temperature as Lost Spring. Both springs emerge from Sims Butte lava, and the seasonally fluctuating water table may sometimes be below White Branch Spring while always providing flow to Lost Spring.

4.2. Flow Path Depths and Helium Sources

[43] In order to aid comparison of helium isotope ratios reported in this paper with those collected from other hot and cold springs in the region, helium isotope ratios were adjusted following the air-saturated water corrections of *Hilton* [1996] despite the possibility that the highly atmospheric signature of the spring water may dilute the magmatic helium signal [*Saar et al.*, 2005]. For the springs sampled in this study, measured R/R_a values range from 0.93 to 2.14, and corrected ratios (R_c/R_a) range from 0.74 to 3.19 (Table 3). The helium isotope ratios are similar to those

Table 3. Tritium-Helium Data, Helium Sources, and Residence Time Estimates

	Great	Lost	Olallie North	Olallie South	Roaring	Tamolitch
^{3}H, TU	3.83	3.57	4.18	4.38	4.67	4.61
^{4}He$_{meas}$, cm^3/g STP	1.14×10^{-7}	1.10×10^{-7}	3.37×10^{-7}	6.74×10^{-8}	7.29×10^{-8}	6.41×10^{-8}
Ne$_{meas}$, cm^3/g STP	2.55×10^{-7}	2.33×10^{-7}	5.20×10^{-7}	2.13×10^{-7}	2.78×10^{-7}	2.27×10^{-7}
(^{3}He/^{4}He)$_{meas}$/R$_a$	1.16	2.14	0.93	1.14	0.96	1.08
(^{3}He/^{4}He)corr/R$_a$	1.32	3.19	0.90	1.48	0.74	1.38
^{3}H/^{3}He mean transit time, years	26.0	54.5	20.3[a]	16.5	4.1[b]	11.4
Lower uncertainty limit	25.5	54.0	19.8	16.1	3.4	10.9
Upper uncertainty limit	26.5	55.1	20.7	16.9	4.1	11.7
Exponential mean transit time, years	13.3		10.1	8.7	4.4	7.1
Lower uncertainty limit	12.9		9.9	8.6	4.0	7.0
Upper uncertainty limit	13.7		10.3	8.9	4.4	7.2
Gamma mean transit time, years	13.6		8.7	7.0	3.2	5.4
Lower uncertainty limit	12.9		8.4	6.8	2.9	5.2
Upper uncertainty limit	14.4		8.9	7.1	3.2	5.4

[a]Entrapment of an air bubble during sampling yielded spurious results; ^{3}He$_{trit}$ was estimated from interpolation between Olallie South Spring and Great Spring values, based on their ^{3}H measurements.
[b]Calculated (^{3}He/^{4}He)$_{terr}$ yielded a negative age; (^{3}He/^{4}He)$_{terr}$ of 0.007 (crustal end-member) was used to calculate ^{3}He$_{trit}$.

of cold springs on the east side of the Cascades, which range from 0.95 to 5.19 R$_c$/Ra [*Saar et al.*, 2005]. Three geothermal springs in the McKenzie River watershed have ^{3}He/^{4}He ratios of 3.3 to 5.2 R$_c$/Ra, and cold springs feeding Separation Creek, a tributary to the McKenzie River have the highest ratios reported in the Cascades, ranging from 2.4 to 8.6 R$_c$/Ra [*Evans et al.*, 2004]. The high helium isotope ratios in the Separation Creek springs are the result of magmatic degassing from an intrusion underlying the area [*Evans et al.*, 2004]. We infer that R/R$_a$ values >1 in our study area are related to magmatic gas emissions.

[44] Olallie South, Tamolitch, and Roaring springs have helium isotope ratios close to that of the atmosphere and have little ^{3}He from terrigenic sources (crustal and magmatic). These springs likely follow shallow flow paths where they encounter a low terrigenic helium flux in their short transit time. Underlying these shallow flow paths, there may be deep geothermal water that incorporates the terrigenic helium, shielding the cold springs from encountering it (Figure 2). The Ne/^{4}He ratio for Olallie North suggests that entrapment of an air bubble during sampling yielded spurious results. ^{3}He$_{trit}$ for Olallie North was estimated from interpolation between Olallie South Spring and Great Spring values, based on their ^{3}H measurements.

[45] Lost Spring has the largest discharge and largest mantle component of any of the sampled springs. These results conform to the model of regional groundwater systems with longer transit times and higher ^{3}He/^{4}He ratios than more localized aquifers [*James et al.*, 2000; *Nathenson and Thompson*, 2003; *Saar et al.*, 2005]. Perhaps more importantly, the aquifer feeding Lost Spring crosses the White Branch Fault Zone [*Conrey et al.*, 2002], where a water supply well is slightly thermal, with an elevated chloride concentration (56 mg/L) and R$_c$/R$_a$ value (6.8) [*Evans et al.*, 2004]. We suggest that, in the vicinity of the fault zone, groundwater with near-atmospheric helium ratios mixes with a small amount of thermal water with a magmatic helium isotope signature. This results in the helium isotope ratios sampled downgradient at Lost Spring. This interpretation is supported by the low ^{14}C values for the well and Lost Spring [*Evans et al.*, 2004] and may also explain the anomalously warm temperature of Lost Spring

as compared to that of its recharge elevation. These results suggest that fault zones play a key role in mixing deep geothermal water with shallow groundwater systems.

4.3. Transit Time

[46] Using the tritium-tritogenic helium data, mean transit times for the spring aquifers were estimated in three ways (Table 3). Transit times calculated using the ratio of ^{3}H/^{3}He (equation (4)), range from 4.1 years for Roaring Spring to 26.0 years for Great Spring. Transit times derived using the exponential (equation (5)) and gamma (equation (6)) distributions are shorter, ranging from 4.4 to 13.3 years and from 3.2 to 13.6 years respectively. Uncertainty surrounding each estimate is ∼1 year.

[47] The simple exponential and gamma distributions, which apply to flow through porous media, may not reflect the complex hydrogeology of the study area. If there is significant flow through interconnected fractures or zones of stagnant water, tracer-based transit time estimates may not reflect the water's true transit time and multiple tracers may provide divergent estimates [*Mazor and Nativ*, 1992; *Maloszewski et al.*, 2004]. Other models that include dual porosity systems [e.g., *Maloszewski and Zuber*, 1985] might better represent the physical conditions. However, these models require more complete information about fracture geometry and matrix characteristics than are available for the study area. *Cook et al.* [2005] showed that it may be possible to constrain fracture and matrix parameters by measuring multiple tracers in vertically nested piezometers. However, mixing of multiple flow lines occurs at the springs, so no tracer profiles can be derived, nor fracture parameters determined, in the High Cascades. Many studies have simplified matters by treating the aquifer as a porous matrix and ignoring the fractures [*Aeschbach-Hertig et al.*, 1998; *Manga*, 1999]. In such models, the aquifer is represented by a single hydraulic conductivity reflecting contributions from both fractures and matrix. This is the approach taken here.

[48] The exponential and gamma models produce similar results, with Great Spring having slightly longer transit times and the other springs having slightly shorter transit times in the gamma model than in the exponential model.
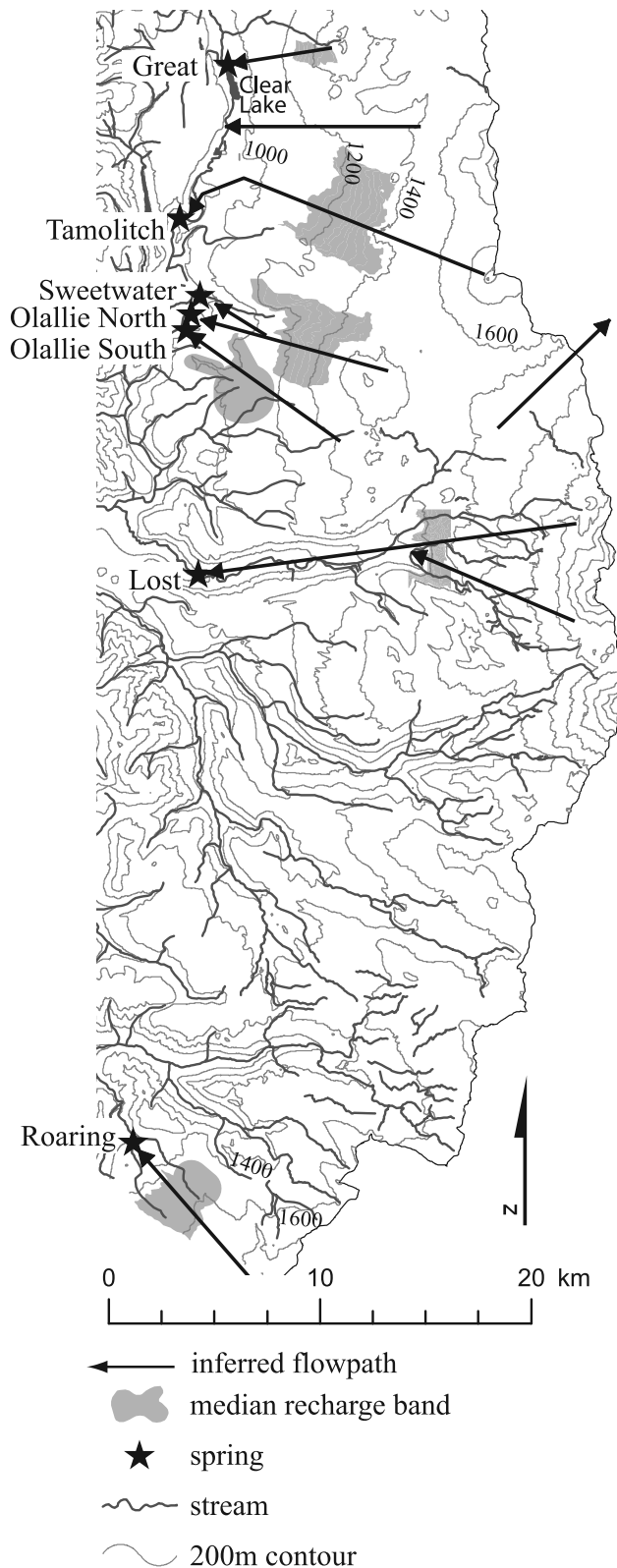
Figure 8. Surface topography, inferred groundwater flow paths, and recharge areas, based on geology and estimated recharge elevation and area. Cascade crest forms eastern edge of the map.

Without repeated sampling, it is impossible to determine which model is more appropriate for the spring systems studied, so we choose to bracket the transit times using the shortest and longest times from the two models for each spring. Thus transit time to Great Spring averages 12.9–14.4 years; Olallie North averages 8.4–10.3 years; Olallie South averages 6.8–8.9 years; Roaring averages 2.9–4.4 years; and Tamolitch averages 5.2–7.2 years. For these five springs, the mean transit time is 7.2 years when weighted by discharge.

[49] The long mean transit time for Lost Spring, 54.5 years using the ^{3}H/^{3}He ratio, cannot be explained using the exponential or gamma models. It is probably the result of mixing between groundwater with shorter transit times and deeper, tritium-dead groundwater. This interpretation is consistent with the temperature and helium data discussed above.

5. Discussion

5.1. Recharge Areas

[50] While there are too many possible permutations to fully constrain recharge area geometry without hydraulic head data, isotopic and geologic data allow estimates of the likely size and flow path of each aquifer. Isotopically determined recharge elevations highlight a band across each topographic watershed, from which a mean precipitation value is derived from PRISM data. Spring discharge is multiplied by the regional runoff ratio (0.68) and divided by the mean precipitation to calculate the recharge area for each spring. Overall, the six springs require a recharge area that is 95% of the size of their combined topographic watersheds. However, there are large discrepancies between the estimated size of the recharge area and the size of the topographic watershed for each individual spring (Table 1).

[51] For a portion of the upper McKenzie River watershed in which five major springs are located (453 km^2, Figure 1b), recharge for the springs requires 66% of the area. Most of the remaining area provides water for small runoff-dominated streams and accretion along the McKenzie River channel, while the rest likely drains east of the Cascades crest. A regional groundwater model for the Deschutes River basin, lying east of the McKenzie River basin, requires 22.6 m^3/s of water from the west side of the Cascades crest in order to account for all of the groundwater discharge in that arid environment [*Gannett and Lite*, 2004]. The McKenzie River basin likely supplies <3 m^3/s of water to the east side.

[52] In addition to estimating the area of the groundwater recharge zones, we constrained their locations based on geology and mean recharge elevation (Figure 8). Great Spring is likely sourced on and around Sand Mountain, both within and outside of its topographic watershed. Tamolitch Spring is probably fed by groundwater recharge and flow through Belknap Crater lava, in the southern portion of its watershed, with the rest of the area likely providing the ~6 m^3/s of groundwater that accretes in the McKenzie River channel between Clear Lake and Tamolitch Spring. Scott Mountain appears to be a major area of groundwater recharge. Sweetwater and Olallie North springs are probably sourced in the northern and eastern

portions of Scott Mountain, while Olallie South Spring may derive its water from lower-elevation Scott Mountain lava, within and to the south of its topographic watershed. The likely recharge area for Lost Spring is less clear, although there are a few clear point sources of recharge where streams and lakes drain into the Collier Cone lava. The occurrence of these point sources suggests that the southern portion of the Lost Spring topographic watershed may be the source of the spring's water. The area bounded on the north by Sims Butte and Collier Cone lava supplies more than enough water to account for the spring's discharge. The northern portion of the watershed may drain to the more northerly springs and may also provide water to the Deschutes basin. Roaring Spring is probably sourced along the Cascade Crest, but glacial and erosional processes in the >120,000 years since lava emplacement obscure lava geometries and confound specific interpretations of the recharge area.

5.2. Aquifer Properties

[53] The Quaternary lavas of the High Cascades are exposed over large areas of the landscape surface and, where not exposed, are buried only by shallow soils or glacial deposits. These lavas form a stack of mostly high permeability rock more than 1000 m in thickness, as documented in deep bore holes in the study region [*Conrey et al.*, 2002]. Thermal profiles in the bores holes are isothermal within the uppermost several hundred meters of the saturated zone, which has been attributed to the high transmissivity of groundwater through these aquifers. Analysis of thermal, as well as other data, suggests that hydraulic conductivities are on the order of 10^{-6} m/s at 500 m [*Saar and Manga*, 2004].

[54] Driller's logs for 6 wells drilled in late Quaternary lavas in the study region showed an average rise of 11 m between the depth where water was first encountered and the subsequent static water level (Oregon Water Resources Department, Well Log Database, http://apps2.wrd.state.or.us/apps/gw/well_log/Default.aspx/). Only one well had a static water level at the same depth as it was first discovered. One well became artesian when drillers reached a depth of 17 m. These drill logs suggest that much of the High Cascades aquifer system behaves as a confined aquifer.

[55] The volume of mobile water in an aquifer is the product of the mean transit time and spring discharge (*Q*). Using 7.2 years as the mean transit time and a total discharge of 17.07 m³/s from the seven springs, combined mobile water volume is ~4 km³. The aquifer thickness can then be calculated by dividing the aquifer volume by its porosity and mass balanced recharge area. We assume an effective porosity of 15%, following *Ingebritsen et al.* [1994], and calculate aquifer thicknesses ranging from ~30 m for Roaring Spring to ~120 m for Great Spring. Seepage velocities were calculated from the effective porosity multiplied by the distance between the spring and the mean recharge elevation band divided by the mean transit time. Seepage velocities range between 1×10^{-6} and 7×10^{-6} m/s (0.1 to 0.6 m/d).

[56] Assuming groundwater flow through a homogeneous, isotropic porous material, we use Darcy's law,

$$K = \frac{Q}{bw}\frac{dl}{dh},\qquad(8)$$

to determine the hydraulic conductivity of our investigated volcanic aquifers in the High Cascades. Here *K* is hydraulic conductivity, *dl* is the distance between the spring and its mean recharge elevation band, *dh* is the elevation difference between mean recharge and the spring, *w* is the width of the lava flow from which the spring emerges in a cross section near the spring, and *b* is the aquifer thickness. Calculated hydraulic conductivities are $3 \times 10^{-4} \le K \le 1 \times 10^{-2}$ m/s. These results bracket an estimated hydraulic conductivity on the order of 10^{-3} m/s for springs in the Deschutes River basin, directly to the east of the study area, derived from a linearized Boussinesq equation for unconfined aquifers [*Manga*, 1996]. They also bracket an estimated hydraulic conductivity of 2×10^{-3} m/s for a spring near Lassen, part of the California Cascades, made using the Boussinesq equation in combination with spring-fed stream recession analysis and mean transit time from ^{3}H/^{3}He [*Manga*, 1999]. Basalt flows on Kilauea, Hawaii, also have very similar hydraulic conductivities [*Ingebritsen and Scholl*, 1993].

6. Conclusions

[57] In young volcanic arcs that receive large amounts of annual precipitation, high recharge rates coupled with volcanic aquifers that have high near-surface hydraulic conductivity lead to extensive groundwater systems. The aquifers are locally constrained by the geographic extent of permeable lava flows, with recharge areas and flow paths that are not fully bounded by modern topography. Flow paths are generally shallow and water discharging at large, cold springs has had limited contact with geothermal systems. A combination of hydrologic, isotopic, and geologic data illuminate these groundwater systems by providing data on aquifer sizes and locations, recharge elevations, transit times, and other aquifer characteristics. Our observations on the west slope of the Oregon High Cascades emphasize the importance of volcanic history in controlling the patterns of groundwater flow in young mafic landscapes.

References

Aeschbach-Hertig, W., P. Schlosser, M. Stute, H. J. Simpson, A. Ludin, and J. F. Clark (1998), A ^{3}H/^{3}He study of ground water flow in a fractured bedrock aquifer, *Ground Water*, *36*(4), 661–670.

Aharonson, O., M. T. Zuber, D. H. Rothman, N. Schorghofer, and K. X. Whipple (2002), Drainage basins and channel incision on Mars, *Proc. Natl. Acad. Sci. U. S. A.*, *99*(4), 1780–1783.

Bowen, G. J., and B. Wilkinson (2002), Spatial distribution of δ^{18}O in meteoric precipitation, *Geology*, *30*(4), 315–318.

Carter, R. W., and J. Davidian (1968), General procedure for gaging streams, *U.S. Geol. Surv. Tech. Water Resour. Invest., Book 3 Chap. A6.*

Clarke, W. B., W. J. Jenkins, and Z. Top (1976), Determination of tritium by mass-spectrometric measurement of ^{3}He, *Int. J. Appl. Radiat. Isotopes*, *27*, 515–522.

Coleman, M. L., T. J. Sheperd, J. J. Durham, J. E. Rouse, and G. R. Moore (1982), Reduction of water with zinc for hydrogen isotope analysis, *Anal. Chemi.*, *54*, 993–995.

Conrey, R. M., D. R. Sherrod, P. Hooper, and D. Swanson (1997), Diverse primitive magmas in the Cascade arc, northern Oregon and southern Washington, *Can. Mineral.*, *35*, 367–396.

Conrey, R. M., E. M. Taylor, J. M. Donnely-Nolan, and D. R. Sherrod (2002), North-central Oregon Cascades: Exploring petrologic and tectonic intimacy in a propagating intra-arc rift, in *Field Guide to Geologic Processes in Cascadia*, edited by G. W. Moore, pp. 47–90, Oregon Dep. of Geol. and Miner. Ind., Salem.

Cook, P. G., A. J. Love, N. I. Robinson, and C. T. Simmons (2005), Groundwater ages in fractured rock aquifers, *J. Hydrol.*, *308*(1–4), 284–301.

Craig, H. (1961), Isotopic variations in meteoric waters, *Science*, *133*, 1702.

Daly, C., R. P. Nielson, and D. L. Phillips (1994), A statistical-topographic model for mapping climatological precipitation over mountainous terrain, *J. Appl. Meteorol.*, *33*, 140–158.

Daly, C., W. P. Gibson, G. H. Taylor, G. L. Johnson, and P. Pasteris (2002), A knowledge-based approach to the statistical mapping of climate, *Clim. Res.*, *22*, 99–113.

Dansgaard, W. (1964), Stable isotopes in precipitation, *Tellus*, *16*(4), 436–468.

Davis, S. N. (1969), Porosity and permeability of natural materials, in *Flow Through Porous Media*, edited by R. J. M. De Wiest, pp. 53–89, Elsevier, New York.

Descloitres, M., M. Ritz, B. Robineau, and M. Courteaud (1997), Electrical structure beneath the eastern collapsed flank of Piton de la Fournaise volcano, Reunion Island: Implications for the quest for groundwater, *Water Resour. Res.*, *33*(1), 13–19.

Epstein, S., and T. Mayeda (1953), Variation of ^{18}O content of water from natural sources, *Geochim. Cosmochim. Acta*, *4*, 213–224.

Etcheverry, D., and P. Perrochet (2000), Direct simulation of groundwater transit-time distributions using the reservoir theory, *Hydrogeology J.*, *8*, 200–208.

Evans, W. C., M. C. van Soest, R. H. Mariner, S. Hurwitz, S. E. Ingebritsen, C. W. J. Wicks, and M. E. Schmidt (2004), Magmatic intrusion west of Three Sisters, central Oregon, USA: The perspective from spring geochemistry, *Geology*, *32*(1), 69–72.

Gannett, M. W., and K. E. J. Lite (2004), Simulation of regional groundwater flow in the upper Deschutes Basin, Oregon, *U.S. Geol. Surv. Water Res. Invest. Rep.*, *03-4195*.

Gannett, M. W., M. Manga, and K. E. J. Lite (2003), Groundwater hydrology of the Upper Deschutes Basin and its influence on streamflow, in *A Peculiar River: Geology, Geomorphology, and Hydrology of the Deschutes River, Oregon*, *Water Sci. Appl. Ser.*, vol. 7, edited by J. E. O'Connor and G. E. Grant, pp. 31–49, AGU, Washington, D. C.

Hayhoe, K., et al. (2004), Emissions pathways, climate change, and impacts on California, *Proc. Natl. Acad. Sci. U. S. A.*, *101*(34), 12,422–12,427.

Head, J. W., L. Wilson, and K. L. Mitchell (2003), Generation of recent massive water floods at Cerberus Fossae, Mars by dike emplacement, cryospheric cracking, and confined aquifer groundwater release, *Geophys. Res. Lett.*, *30*(11), 1577, doi:10.1029/2003GL017135.

Herrett, T. A., G. W. Hess, J. G. House, G. P. Ruppert, and M.-L. Courts (2004), Water resources data for Oregon, water year 2004, *U.S. Geol. Surv. Water Data Rep., OR-04-1*, 968 pp.

Hilton, D. R. (1996), The helium and carbon systematics of a continental geothermal system: Results from monitoring studies at Long Valley Caldera (California, U.S.A.), *Chem. Geol.*, *127*, 269–295.

Ingebritsen, S. E., and M. A. Scholl (1993), The hydrogeology of Kilauea volcano, *Geothermics*, *22*, 255–270.

Ingebritsen, S. E., R. H. Mariner, and D. R. Sherrod (1994), Hydrothermal systems of the Cascade Range, north-central Oregon, *U.S. Geol. Surv. Prof. Pap.*, *1044-L*, 86 pp.

Izuka, S. K., and S. B. Gingerich (2003), A thick lens of fresh groundwater in the southern Lihue Basin, Kauai, Hawaii, USA, *Hydrogeol. J.*, *11*, 240–248.

James, E. R., M. Manga, T. P. Rose, and G. B. Hudson (2000), The use of temperature and isotopes of O, H, C and noble gases to determine the pattern and spatial extent of groundwater flow, *J. Hydrol.*, *237*(1–2), 100–112.

Jefferson, A., G. E. Grant, S. L. Lewis, and C. Tague (2004), Geology broadly predicts summer streamflow in volcanic terrains: Lessons from the Oregon Cascades, *Eos Trans. AGU*, *85*(47), Fall Meet. Suppl., Abstract H33C-0475.

Join, J.-L., J.-L. Folio, and B. Robineau (2005), Aquifers and groundwater within active shield volcanoes: Evolution of conceptual models in the Piton de la Fournaise volcano, *J. Volcanol. Geotherm. Res.*, *147*(1–2), 187–201.

Kiernan, K., C. Wood, and G. Middleton (2003), Aquifer structure and contamination risk in lava flows: Insights from Iceland and Australia, *Environ. Geol.*, *43*, 852–865.

Kilburn, C. R. J. (2000), Lava flows and flow fields, in *Encyclopedia of Volcanoes*, edited by H. Sigurdsson, pp. 291–305, Elsevier, New York.

Kirchner, J. W., X. Feng, and C. Neal (2001), Fractal stream chemistry and its implications for contaminant transport in catchments, *Nature*, *403*, 524–527.

Lund, E. H. (1977), Geology and hydrology of the Lost Creek glacial trough, *Ore Bin*, *39*(9), 141–156.

Maloszewski, P., and A. Zuber (1985), On the theory of tracer experiments in fissured rocks with a porous matrix, *J. Hydrol.*, *79*, 333–358.

Maloszewski, P., W. Stichler, and A. Zuber (2004), Interpretation of environmental tracers in groundwater systems with stagnant water zones, *Isotopes Environ. Health Stud.*, *40*, 21–33.

Manga, M. (1996), Hydrology of spring-dominated streams in the Oregon Cascades, *Water Resour. Res.*, *32*(8), 2435–2440.

Manga, M. (1997), A model for discharge in spring-dominated streams and implications for the transmissivity and recharge of quaternary volcanics in the Oregon Cascades, *Water Resour. Res*, *33*(8), 1813–1822.

Manga, M. (1998), Advective heat transport by low-temperature discharge in the Oregon Cascades, *Geology*, *26*(9), 799–802.

Manga, M. (1999), On the timescales characterizing groundwater discharge at springs, *J. Hydrol.*, *219*, 56–69.

Manga, M., and J. W. Kirchner (2004), Interpreting the temperature of water at cold springs and the importance of gravitational potential energy, *Water Resour. Res.*, *40*, W05110, doi:10.1029/2003WR002905.

Mazor, E., and R. Nativ (1992), Hydraulic calculation of groundwater flow velocity and age: Examination of the basic premises, *Hydrol. J.*, *138*, 211–222.

McGuire, K. J., J. J. McDonnell, M. Weiler, C. Kendall, B. L. McGlynn, J. M. Welker, and J. Seibert (2005), The role of topography on catchment-scale water residence time, *Water Resour. Res.*, *41*, W05002, doi:10.1029/2004WR003657.

Michel, R. L. (1989), Tritium deposition in the continental United States: 1953–1983, *U.S. Geol. Surv. Water Res. Invest. Rep.*, *89-4072*.

Mote, P. W., A. F. Hamlet, M. Clark, and D. P. Lettenmaier (2005), Declining mountain snowpack in western North America, *Bull. Am. Meteorol. Soc.*, *86*(1), 39–49.

Nathenson, M., and J. M. Thompson (2003), Slightly thermal springs and non-thermal springs at Mount Shasta, California: Chemistry and recharge elevations, *J. Volcanol. Geotherm. Res.*, *121*, 137–153.

Rademacher, L. K., J. F. Clark, D. W. Clow, and G. B. Hudson (2005), Old groundwater influence on stream hydrochemistry and catchment response times in a small Sierra Nevada catchment: Saheghen Creek, California, *Water Resour. Res.*, *41*, W02004, doi:10.1029/2003WR002805.

Revil, A., A. Finizola, F. Sortina, and M. Ripepe (2004), Geophysical investigations at Stromboli volcano, Italy: Implications for ground water flow and paroxysal activity, *Geophys. J. Int.*, *157*, 426–440.

Rose, T. P., M. L. Davisson, and R. E. Criss (1996), Isotope hydrology of voluminous cold springs in fractured rock from an active volcanic region, northeastern California, *J. Hydrol.*, *179*, 207–236.

Saar, M. O., and M. Manga (2004), Depth dependence of permeability in the Oregon Cascades inferred from hydrogeologic, thermal, seismic, and magmatic modeling constraints, *J. Geophys. Res.*, *109*, B04204, doi:10.1029/2003JB002855.

Saar, M. O., M. C. Castro, C. M. Hall, M. Manga, and T. P. Rose (2005), Quantifying magmatic, crustal, and atmospheric helium contributions to volcanic aquifers using all stable noble gases: Implications for magmatism and groundwater flow, *Geochem. Geophys. Geosyst.*, *6*, Q03008, doi:10.1029/2004GC000828.

Schlosser, P., M. Stute, C. Sonntag, and K. O. Munnich (1989), Tritogenic ^{3}He in shallow groundwater, *Earth Planet. Sci. Lett.*, *94*, 245–256.

Scott, W. E. (1977), Quaternary glaciation and volcanism, Metolius River area, Oregon, *Geol. Soc. Am. Bull.*, *88*, 113–124.

Sherrod, D. R. (1991), Geologic map of a part of the Cascade Range between latitudes 43°–44°, central Oregon, *U.S. Geol. Surv. Misc. Invest. Ser.*, *I-1891*.

Sherrod, D. R., and J. G. Smith (1990), Quaternary extrusion rates of the Cascade Range, northwestern United States and southern British Columbia, *J. Geophys. Res.*, *95*, 19,465–19,474.

Sherrod, D. R., and J. G. Smith (2000), Geologic Map of upper Eocene to Holocene volcanic and related rocks of the Cascade Range, Oregon, *U. S. Geol. Surv. Geol. Invest. Ser.*, *I-2569*.

Sherrod, D. R., E. M. Taylor, M. L. Ferns, W. E. Scott, R. M. Conrey, and G. A. Smith (2004), Geologic map of the Bend 30- × 60-minute quadrangle, central Oregon, *U.S. Geol. Surv. Geol. Invest. Ser.*, *I-2683*.

Stearns, H. T. (1929), Geology and water resources of the Upper McKenzie Valley, Oregon, *U.S. Geol. Surv. Water Supply Pap.*, *597-D*.

Tague, C., and G. E. Grant (2004), A geological framework for interpreting the low flow regimes of Cascade streams, Willamette River Basin, Oregon, *Water Resour. Res.*, *40*, W04303, doi:10.1029/2003WR002629.

Tague, C., M. Farrell, G. E. Grant, S. Lewis, and S. Rey (2006), Hydrogeologic controls on summer stream temperatures in the McKenzie River basin, Oregon, *Hydrol. Processes*, in press.

Taylor, G. H., and C. Hannan (1999), *The Climate of Oregon: From Rain Forest to Desert*, 211 pp., Oregon State Univ. Press, Corvallis.

———————————

G. Grant, Pacific Northwest Research Station, Forest Service, USDA, Corvallis, OR 97331, USA.

A. Jefferson, Department of Geosciences, Oregon State University, Corvallis, OR USA. (jeffersa@geo.oregonstate.edu)

T. Rose, Chemical Biology and Nuclear Science Division, Lawrence Livermore National Laboratory, Livermore, CA 94550, USA.